IEEE Access
Multidisciplinary ⋮ Rapid Review ⋮ Open Access Journal

Received April 3, 2022, accepted April 28, 2022, date of publication May 3, 2022, date of current version May 9, 2022.

Digital Object Identifier 10.1109/ACCESS.2022.3172338

Fault Diagnosis of the Rotating Rectifier Diode Over a TSSM Based on the Armature Current Calculation and Similarity Measurement

PEIRONG ZHU[1], YONGZHI LIU[2], AND BINGJIE FAN[2]
[1]Graduate School, Air Force Engineering University, Xi'an 710043, China
[2]Aviation Engineering School, Air Force Engineering University, Xi'an 710043, China
Corresponding author: Peirong Zhu (1933968982@qq.com)

ABSTRACT This work proposes a method for detecting the fault of a rotating rectifier. The rotating rectifier is an important part of a three-stage synchronous motor. It is located on the high-speed rotating rotor. The diode in the rectifier is prone to failure owing to the adverse working environment. Our method calculates the rotor armature current of the main exciter, and utilizes the similarity and difference of the current polarity of the three-phase armature current of excitation motor under multiple working states to measure the health status of the rotating rectifier. A similarity measurement algorithm based on the armature current Manhattan distance residual has been proposed, and the fault type and location of the rotating rectifier diode have been found by using the necessary rule for a trade-off. Considering the existence of interference and error, the preset value is employed and compared with the residual function. The results from the experiment have verified the effectiveness of the proposed fault diagnosis method.

INDEX TERMS Rotating rectifier, armature current, Manhattan distance, fault diagnosis.

NOMENCLATURE

U_{egf}	ME excitation voltage, V.
i_{egf}	ME excitation current, A.
R_{egf}	ME stator resistance, Ω.
i_{ear}, i_{ebr}, i_{ecr}	ME armature current, A.
ψ_{egf}	Flux linkage between ME stator and rotor-windings, wb.
L_{egf}	ME stator inductance, H.
M_{af}	Mutual inductance amplitude between ME stator and rotor-windings, H.
θ_e	The electrical angle between ME stator and rotor-windings, rad.
Δ	differential operator.

I. INTRODUCTION

The research over multi (all) electric aircraft has developed rapidly [1] owing to the large number of sophisticated airborne equipment, which mandates advanced requirements for the reliability of the aircraft power supply system [2]. A three-stage synchronous motor (TSSM) is the key equipment of the aircraft main power supply system, and its failure will compromise the flight safety of the aircraft. According to Todd *et al.* [3], [4], by aiming at the possible fault state of TSSM, and obtaining the long state monitoring data combined with the method of quantitative analysis based on hazard degree matrix, rotating rectifiers is generally used as connectors between windings of synchronous motors [5], and the fault frequency of the rotating rectifier becomes the highest for the fault mode of synchronous alternator, and it needs to be given priority. The rotating rectifier is located between the main exciter (ME) and the main generator (MG) of the TSSM (shown in Fig.1). Therefore, to ensure flight safety, it is necessary to diagnose the working state of the rotating rectifier.

The process of fault diagnosis of the rotating rectifier includes the signal acquisition, fault feature extraction, and fault classification. For fault feature extraction and diagnosis methods, the fault diagnosis technology has been divided into three categories by Frank [6], viz., the methods based on analytical model, signal processing, and intelligent algorithms.

According to Sottile *et al.* [7], the working characteristics of the rotating rectifier under various fault modes have been

The associate editor coordinating the review of this manuscript and approving it for publication was S. K. Panda.

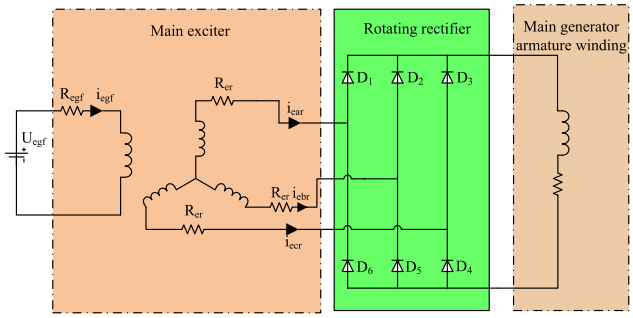

FIGURE 1. Structure of the TSSM.

analyzed. By using Fourier transform to obtain the second harmonic amplitude of the excitation current, a condition monitoring model method of rotating rectifier, based on the excitation current, has been proposed. According to Zouaghi *et al.*. [8], the simulation model of the brushless excitation module has been established. The fault monitoring of the rotating rectifier has been realized by collecting the output voltage signal and diode current signal of the rotating rectifier, besides combining with the corresponding fault mode. According to Huang *et al.*. [9], the Petri net model of the synchronous alternator has been established. By analyzing the relationship between the characteristics and causes of the fault of the rotating rectifier under different fault modes, a fuzzy optimization model based on inverse proposition has been obtained. Concomitantly, the fuzzy optimization equation has been solved by numerical methods to realize the fault diagnosis of rotating rectifier. According to Tantawy *et al*. [10], the method of generator simulation analysis based on the phase domain modeling has been proposed. The observer detects the fault of an aircraft generator rotating rectifier. The above model-based diagnosis methods are challenging, and hence, it is necessary to obtain the motor model accurately. According to Li *et al.*. [11], a detection coil has been installed on the stator of the synchronous alternator. The purpose of the fault diagnosis has been realized through the signal analysis of the induced EMF on the detection coil. According to Ardle *et al.*. [12], [13], first, the excitation current signal of the exciter has been studied, followed by the comparison of the difference of each order harmonic amplitude under multiple fault modes. Finally, the difference of each order harmonic amplitude has been used to realize the fault diagnosis of the rotating rectifier. According to Mohamed *et al.*. [14], [15], the harmonic amplitude has been obtained by the harmonic analysis of the generator output voltage signal, to identify the fault. Although the above methods based on signal analysis can effectively identify faults, they cannot locate the fault location. The intelligent algorithm, owing to its tremendous advances, can be applied for the rotating rectifier fault diagnosis [16]-[18], though a large number of data samples for training have been required in the fault diagnosis based on the intelligent algorithm. Recently, certain scholars have modified their research methods to actualize the fault diagnosis of the rotating rectifier by analyzing the rotor armature current of the ME. The armature current on the rotor cannot be measured directly, though the ME armature current can be calculated through the voltage and flux linkage equation [19]. Certain scholars have realized the fault diagnosis by analyzing the armature current for the fault of the rotating rectifier of the starting generator [20] - [24]. The excitation winding of the ME of the starter generator adopts two-phase or three-phase excitation, and its motor structure is quite different from the ME of the TSSM. Therefore, the voltage and flux linkage equations of the ME for these two structures are different, which also leads to different methods of armature current estimation. However, these approaches based on armature current have an appreciable guiding significance. Meanwhile, for the selection of fault characteristic signals, the method of using THD as the fault characteristic signal proposed needs more time in reference 20. The methods in references 21 and 22 only realize the diagnosis of open circuit fault of rotating rectifier diode. The diagnosis range needs to be improved, and the anti-interference of its diagnosis rules is poor.

When the diode fails, the armature current of the ME will be asymmetric. Therefore, a new method of diode fault diagnosis has been proposed by using Manhattan distance residual to measure the polarity and the similarity between the three-phase armature currents of the ME. First, the armature current expression has been derived to obtain the fault characteristic signal through the voltage and flux linkage equations, on the stator side of the ME. Further, the health status of the rotating rectifier has been measured according to the similarity of the armature current and the variations of the current polarity under multiple working states of the rotating rectifier. By taking into account of the calculation and experimental measurement errors, a pre-defined threshold has been given and compared with the Manhattan distance residual, and the diagnosis rules for the different fault states of the diode have been obtained. Finally, a series of experiments have been carried out to evaluate the proposed theory, which reveals the effectiveness and reliability of the fault diagnosis method.

The study is organized as follows: Section3 details the fault diagnosis theory based on the similarity analysis. Section4 introduces the armature current calculation process of the ME, and analyzes the characteristics of the armature current of the rotating rectifier under multiple working states. The experimental verification has been provided in Section5, and Section6 gives the conclusions of this paper.

II. FAULT DIAGNOSIS THEORY BASED ON SIMILARITY ANALYSIS

The topology of the rectifier bridge is symmetrical when the rotating rectifier works normally. Once the rotating rectifier diode fails, its topology will become asymmetric, and the similarity of the three-phase currents, viz, i_{ear}, i_{ebr}, i_{ecr}, of the ME is different. Therefore, the fault diagnosis can be carried out by measuring the similarity of the armature current.

Concurrently, when the excitation current frequency and the rotor speed of the ME are constant, the period of the armature current of the ME remains constant irrespective of the normal working of the rotating rectifier. The armature current period is defined as T, and the number of current sampling values during a period is N. At sampling time k, the time of the last current sampling point in the past fundamental current cycle is defined as t, and the armature current sample signal during a period is marked as matrix $A(k)$, as shown below.

$$A(k) = \begin{bmatrix} i_{ear}(t)\ i_{ear}(t+1)\ \ldots.\ i_{ear}(t+N-1) \\ i_{ebr}(t)\ i_{ebr}(t+1)\ \ldots.\ i_{ebr}(t+N-1) \\ i_{ecr}(t)\ i_{ecr}(t+1)\ \ldots.\ i_{ecr}(t+N-1) \end{bmatrix} \quad (1)$$

where t is expressed as

$$t = k - N + 1 \quad (2)$$

The number of columns of matrix $A(k)$ represents the number of samples of the single-phase armature current collected in a cycle, marked as the vector $I_x, x \in (a, b, c)$.

$$I_x = \left[i_x(t)\ i_x(t+1)\ \ldots.\ i_x(t+N-1) \right] \quad (3)$$

There is a phase difference between the three-phase armature currents. To measure the relationship between any three-phase armature current through similarity, it is necessary to sort the phase current data collected in a single cycle to obtain the ordered current sequence $I_x, x \in (a, b, c)$.

Subsequent to the data preprocessing, the Manhattan distance between $\tilde{I}_x$ and $\tilde{I}_y$ is found to be same as the result from equation (4), with $x, y = a, b, c; x \neq y \neq z$.

$$MD_{xy} = \frac{\sum_{i=t}^{i=t+N-1} \left| \tilde{I}_x(i) - \tilde{I}_y(i) \right|}{N^*(\tilde{I}_x^{\max} + \tilde{I}_y^{\max})/2} \quad (4)$$

where $\tilde{I}_x^{\max}$ and $\tilde{I}_y^{\max}$ are the maximum value of the vectors $\tilde{I}_x$ and $\tilde{I}_y$.

A preset threshold T_h has been used to measure the similarity between $\tilde{I}_x$ and $\tilde{I}_y$ to reduce the influence of the experimental measurement errors. If MD_{xy} is less than T_h, it can be considered that $\tilde{I}_x$ and $\tilde{I}_y$ are similar, as shown in equation (5).

$$MD_{xy} < T_h \Rightarrow I_x \approx I_y \quad (5)$$

Here, $\tilde{I}_x \approx \tilde{I}_y$ represents the symmetry of the topological structure of the x-arm and y-arm of the rotating rectifier.

By taking into account of the fault diagnosis time and anti-interference, and combined with the motor parameters of this experimental platform, T_h is taken as 0.2.

When the rotating rectifier works in a normal state and its topological structure is in a symmetric state, then any two vectors $\tilde{I}_x$ and $\tilde{I}_y$ are similar, as given in equation (6).

$$\tilde{I}_x \approx \tilde{I}_y, x, y = a, b, c; x \neq y \quad (6)$$

III. THE CALCULATION OF THE ME ARMATURE CURRENT AND THE ANALYSIS OF THE ARMATURE CURRENT CHARACTERISTICS UNDER MULTIPLE FAULT STATES OF ROTATING RECTIFIER

A. THE CALCULATION OF ME ARMATURE CURRENT

In the TSSM, the armature winding of the ME is generally located on the rotor rotating at high speed, and it is impossible to directly detect the three-phase current of the armature winding. Therefore, to obtain the characteristic signal of the armature current, it is necessary to calculate the armature winding current according to the exciter voltage and flux linkage equation.

Considering that the stator winding terminal voltage and flux linkage of the ME are shown in equations (7) and (8).

$$U_{egf} = R_{egf} i_{egf} + \Delta\psi_{egf} \quad (7)$$

$$\psi_{egf} = L_{egf} i_{egf} + M_{fA} i_{ear} + M_{fB} i_{ebr} + M_{fC} i_{ecr} \quad (8)$$

The mutual inductance between the stator winding and the rotor winding can be expressed as

$$\begin{cases} M_{Af} = M_{fA} = M_{af} \cos\theta_e \\ M_{Bf} = M_{fB} = M_{af} \cos(\theta_e - 120^\circ) \\ M_{Cf} = M_{fC} = M_{af} \cos(\theta_e + 120^\circ) \end{cases} \quad (9)$$

Simultaneous equations (7). (8), and (9), are solved to obtain the armature winding current expression as given below

$$\begin{bmatrix} i_{ear} \\ i_{ebr} \\ i_{ecr} \end{bmatrix} = \frac{1}{3M_{af}} \begin{bmatrix} 2y & 0 \\ y & -\sqrt{3}\,y \\ y & \sqrt{3}\,y \end{bmatrix} \begin{bmatrix} \cos\theta_e \\ \sin\theta_e \end{bmatrix} \quad (10)$$

where

$$y = \int (U_{egf} - R_{egf} i_{egf}) dt - L_{egf} i_{egf} \quad (11)$$

B. ANALYSIS OF ARMATURE CURRENT CHARACTERISTICS UNDER DIFFERENT FAULT STATES OF ROTATING RECTIFIER

The fault status of the rotating rectifier includes the short-circuit and open-circuit faults. When a diode is short-circuited, the corresponding phase current will increase sharply, and finally convert the diode to an open state. Therefore, this work primarily studies the open-circuit faults of the single and double diodes of the rotating rectifier.

To analyze the characteristics of the armature current of the ME, a motor model corresponding to the experimental platform has been built in simplorer.

When the rotating rectifier is in a normal state, the three-phase armature current of the main exciter is shown in Fig. 2(a), and the Manhattan distance of the three-phase armature current is shown in Fig. 2(b).

The diagnostic criteria for the normal state of the rotating rectifier can be expressed as

$$\text{normal} \Leftrightarrow MD_{ab} \approx MD_{ac} \approx MD_{bc} < T_h \quad (12)$$

When a single diode is in open circuit (for e.g., D_1 open circuit), D_1 open circuit fault is set at 12ms in the simulation.

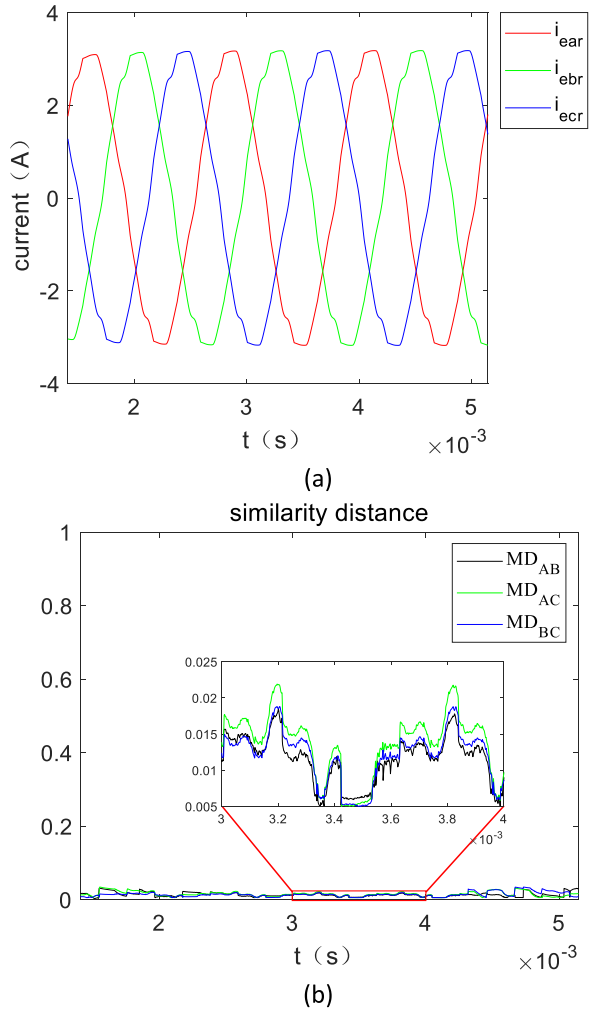

FIGURE 2. Diode normal state (a) Three phase armature current under normal condition (b) Manhattan distance.

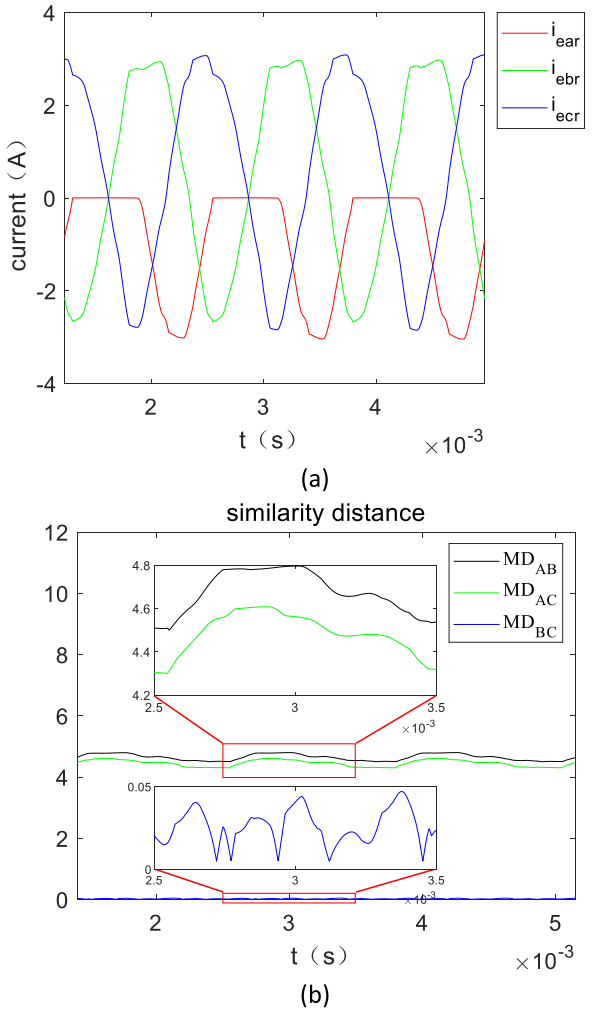

FIGURE 3. D_1 open circuit state (a) Three phase armature current when D1 is open circuit (b) Manhattan distance.

The ME armature current is shown in Fig. 3(a). Concurrently, the Manhattan distance of the armature current is shown in Fig. 3 (b). Fig. 3 (b) shows that the faulty bridge arm is the A bridge arm. This paper analyzes the current polarity of each bridge arm to accurately determine whether the open-circuit diode is in the upper bridge arm or the lower bridge arm. Define Ave to represent the average value of current sampling points in a current period T, as given below

$$Ave_x = \frac{1}{L}\sum_{t=k}^{k+N-1} i_x(t), x = a, b, c \tag{13}$$

When D_1 is open, the following equation is satisfied.

$$Ave_{\mathrm{a}} < 0, Ave_{\mathrm{b}} \approx Ave_{\mathrm{c}} \approx 0 \tag{14}$$

Finally, the fault diagnosis criteria of D_1 open circuit are shown in (15).

$$D_1\text{open circuit} = \begin{cases} MD_{ab} \approx MD_{ac} > T_h \\ Ave_a < 0, Ave_b \approx Ave_c \approx 0 \end{cases} \tag{15}$$

When two diodes are in open circuit (taking the D_1 and D_6 open circuits as the example), the D_1 and D_6 open circuit faults are set at 12 ms in the simulation. The ME armature current is shown in Fig. 4 (a). Concurrently, the Manhattan distance of the ME armature current is shown in Fig. 4 (b). The diagnostic criteria for the D_1 and D_6 open circuits are shown in (16).

$$\mathrm{D_1 and\ D_6 open\ circuit} = \begin{cases} MD_{ab} \approx MD_{ac} > T_h \\ Ave_a \approx Ave_b \approx Ave_c \approx 0 \end{cases} \tag{16}$$

In the normal state, the D_1 open circuit and the D_1 and D_6 open circuit states of the rotating rectifier, are defined with 1, 2, and 3, respectively. Finally, the open circuit fault diagnosis of the rotating rectifier diode is obtained, and the details are listed in Table 1.

IV. EXPERIMENTAL EVALUATIONS

A. THE CALCULATION OF ME ARMATURE CURRENT

Since the TSSM is an integral platform, it is impossible to disassemble and set the diode fault state of the rotating rectifier. In this experiment, an electrically excited synchronous

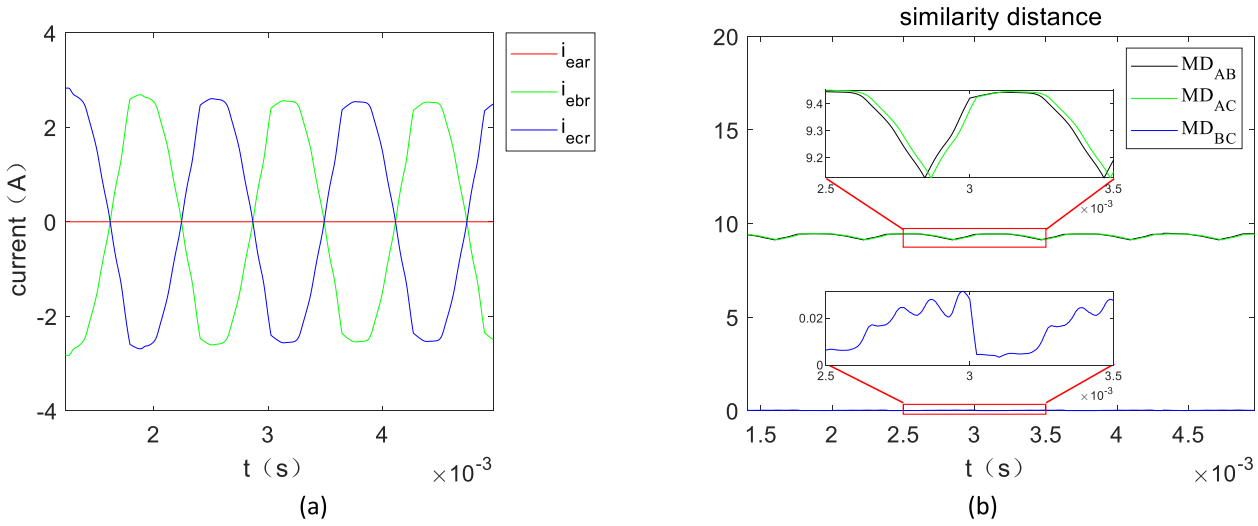

FIGURE 4. D_1 and D_6 open circuit state (a) Three phase armature current when D_1 and D_6 is open circuit (b) Manhattan distance.

TABLE 1. Diode open circuit fault lookup table.

Manhattan distance	Average current	System status	Fault diode	Identification type
$MD_{ab} \approx MD_{ac} \approx MD_{bc} < T_h$	$Ave_a \approx Ave_b \approx Ave_c \approx 0$	0	normal	1
$MD_{ab} \approx MD_{ac} > T_h$ $MD_{bc} < T_h$	$Ave_a < 0$ $Ave_b \approx Ave_c \approx 0$	1	D_1	2
$MD_{ab} \approx MD_{ac} > T_h$ $MD_{bc} < T_h$	$Ave_a \approx Ave_b \approx Ave_c \approx 0$	1	D_1 D_6	3

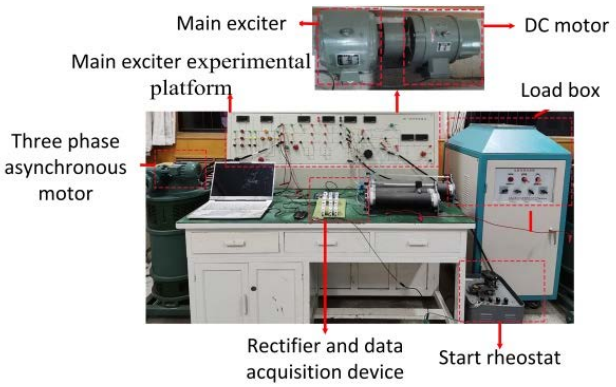

FIGURE 5. Experimental platform.

motor with slip rings have been used to simulate the ME. Due to the slip rings, the main exciter armature current can be directly measured in the experiment. The basic parameters of the ME are shown in Table 2. The inductive (resistive) loads, R=1.4 Ω and L = 23.25 mH, have been used to simulate the excitation winding of the MG. The bridge rectifier is self-made. A switch is connected in series with each diode on the whole bridge, and the fault state of the diode is set by controlling the on and off modes of the switch.

According to the current acquisition scheme, three Hall current sensors have been installed at the output of the ME,

TABLE 2. The basic parameters of the ME.

Parameters	Values
Stator resistor (R_{esf})	1.56Ω
Stator inductance (L_{esf})	286mH
Rotor inductance (L_{esr})	0.335mH
Mutual inductance (M_{af})	3.568mH

and the three-phase armature current of the excitation motor is sampled through the NI USB-6002 with a sampling frequency of 50 ks/s. The final experimental platform is shown in Figure 5.

B. FAULT FREE OPERATION

Figs. 6 (a) and (d) respectively show the measured and calculated armature currents of the ME under the normal state of the rotating rectifier. It can be seen from the figure that the actual armature current of the ME is in good agreement with the calculated armature current of the ME. Figs. 6(b) and (e) show the similarity between the actual main exciter armature current measured by Manhattan distance and the calculated main exciter armature current, respectively, and

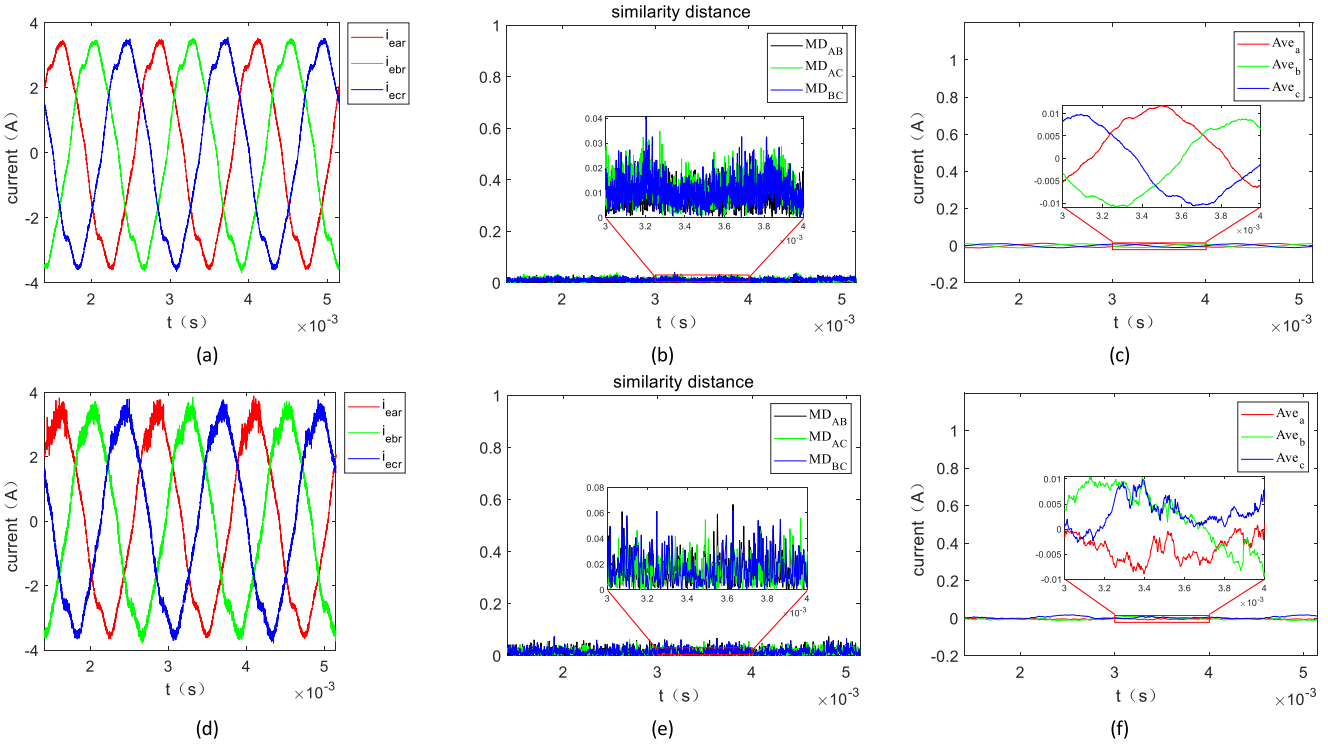

FIGURE 6. Diode normal state (a) Measured three phase armature current (b) Manhattan distance of the measured armature current (c) Average value of the measured armature current (d) Calculated three phase armature current (e) Manhattan distance of the calculated armature current (f) Average value of the calculated armature current

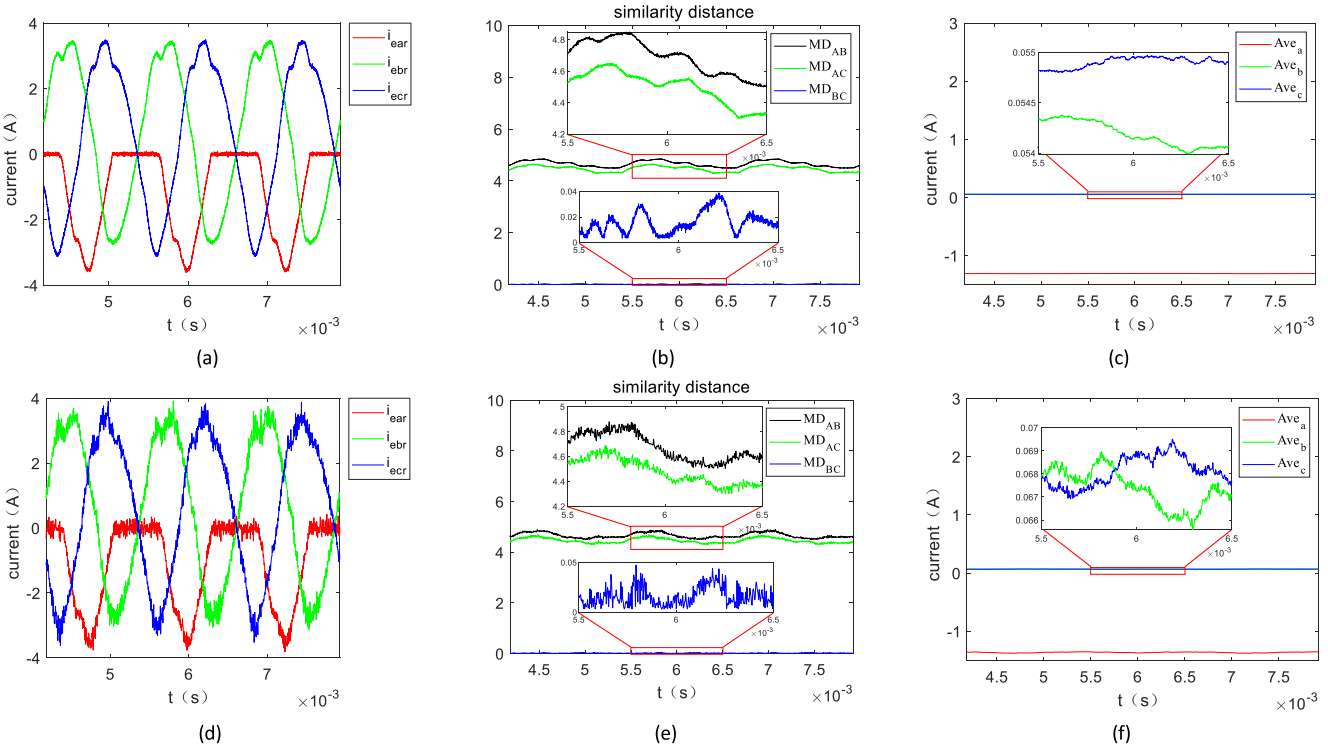

FIGURE 7. D_1 open circuit state (a) Measured three phase armature current (b) Manhattan distance of the measured armature current (c) Average value of the measured armature current (d) Calculated three phase armature current (e) Manhattan distance of the calculated armature current (f) Average value of the calculated armature current.

Figs. 6(c) and (f) respectively show the average value of each bridge arm current.

It can be seen from Fig. 6 that the Manhattan distance, $MD_{ab} \approx MD_{ac} \approx MD_{bc} < T_h$ and $Ave_a \approx Ave_b \approx Ave_c \approx 0$.

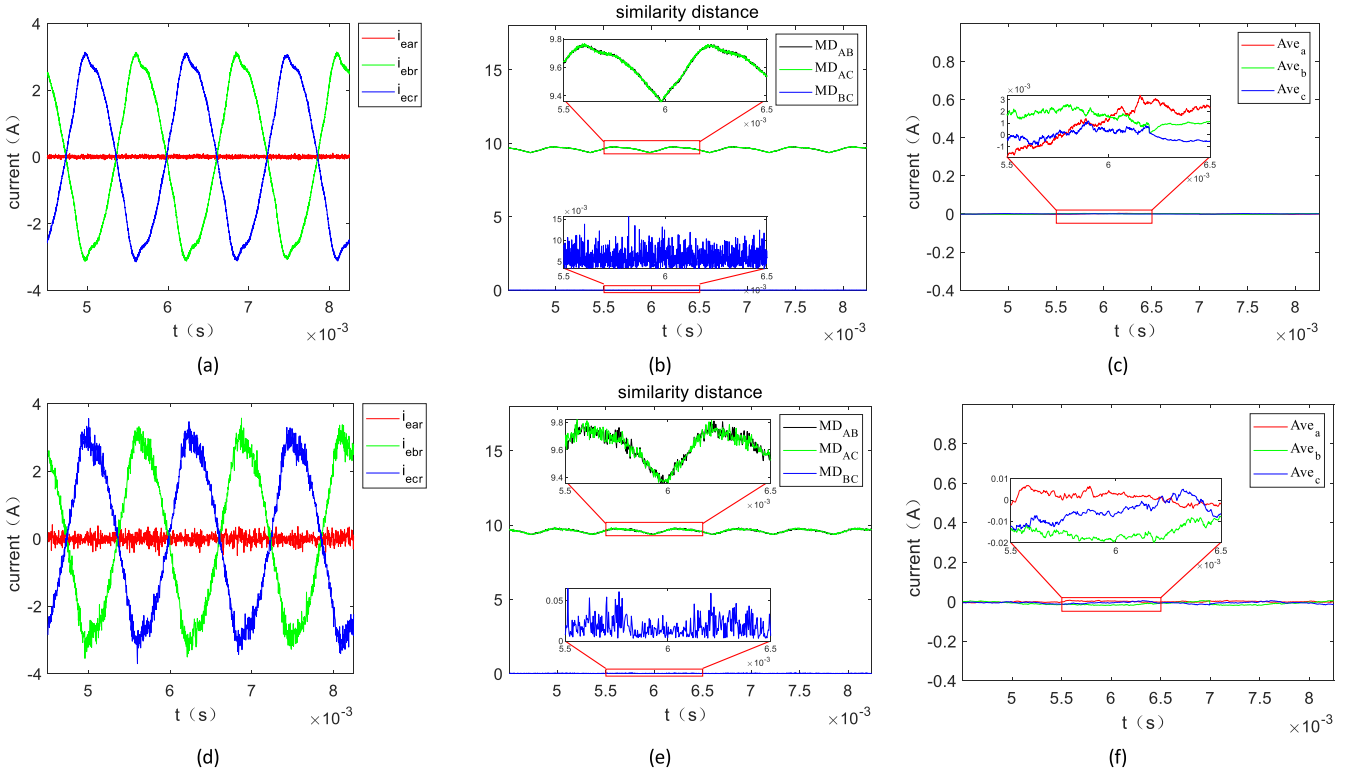

FIGURE 8. D_1 and D_6 open circuit state (a) Measured three phase armature current (b) Manhattan distance of the measured armature current (c) Average value of the measured armature current (d) Calculated three phase armature current (e) Manhattan distance of the calculated armature current (f) Average value of calculated armature current.

According to the diode open circuit fault lookup table 1, the rotating rectifier is in the normal working state at this time.

C. SINGLE DIODE OPEN CIRCUIT FAULT

Figs. 7 (a) and (d) show the measured armature current of the ME and the calculated armature current of the main exciter when the D_1 diode is open circuit. Figs. 7 (b) and (e) show the similarity between the actual main exciter armature current measured by Manhattan distance, and the calculated main exciter armature current, respectively, and Figs. 7 (c) and (f) show the average value of the fault bridge arm current.

It can be seen from Fig 7 that the Manhattan distance $MD_{\text{ab}} \approx MD_{\text{ac}} > T_h, MD_{\text{bc}} < T_h, Ave_a < 0, Ave_b \approx Ave_c \approx 0$. According to the fault diagnosis table 1, the rotating rectifier bridge arm a is in fault state and the D_1 of the upper bridge arm is open circuit.

D. OPEN CIRCUIT FAULTS IN MULTIPLE DIODE

Figs. 8 (a) and (d) show the measured armature currents of the main exciter and the calculated armature current of the ME, when the D_1 and D_6 is open circuit. Figs. 8 (b) and (e) show the similarity between the actual and calculated ME armature currents measured by Manhattan distance and the calculated ME armature current, and Figs. 8 (c) and (f) show the average values of the fault bridge arm currents.

It can be seen from Fig. 8 that the Manhattan distance $MD_{ab} \approx MD_{ac} > T_h, MD_{bc} < T_h, Ave_a \approx Ave_b \approx Ave_c \approx 0$. According to the fault diagnosis table 1, the rotating rectifier bridge arm a is in the fault state and both the diodes, D1 and D6, of the bridge arm a are in open circuit.

V. CONCLUSION

The research over the diode fault diagnosis of the rotating rectifier is of tremendous significance to improve the stability of the power supply system. Here, a fault diagnosis method based on the armature current similarity analysis is proposed in this paper. The experimental results demonstrate that by estimating the armature current of the ME, and analyzing the similarity between the three-phase armature currents and the average value of the bridge arm current, it can distinguish the different working states of the rotating rectifier and identify the fault type. Furthermore, it can accurately locate the position of the fault diode, which proves the effectiveness and superiority of this method.

REFERENCES

[1] S. Huang, L. Xu, Y. Guo, Y. Li, and W. Deng, "Research on three-phase four-leg matrix converter based more electric aircraft wing ice protection system," *J. Eng.*, vol. 2018, no. 13, pp. 529–533, Jan. 2018.

[2] V. Madonna, P. Giangrande, and M. Galea, "Electrical power generation in aircraft: Review, challenges, and opportunities," *IEEE Trans. Transport. Electrific.*, vol. 4, no. 3, pp. 646–659, Sep. 2018.

[3] T. D. Batzel and D. C. Swanson, "Prognostic health management of aircraft power generators," *IEEE Trans. Aerosp. Electron. Syst.*, vol. 45, no. 2, pp. 473–482, Apr. 2009.

[4] T. D. Batzel, D. C. Swanson, and J. F. Defenbaugh, "Predictive diagnostics for the main field winding and rotating rectifier assembly in the brushless synchronous generator," in *Proc. 4th IEEE Int. Symp. Diag. Electr. Mach., Power Electron. Drives (SDEMPED)*, Aug. 2003, pp. 349–354.
[5] S. S. H. Bukhari, G. J. Sirewal, M. Ayub, and J.-S. Ro, "A new small-scale self-excited wound rotor synchronous motor topology," *IEEE Trans. Magn.*, vol. 57, no. 2, pp. 1–5, Feb. 2021.
[6] P. M. Frank, "Analytical and qualitative model-based fault diagnosis—A survey and some new results," *Eur. J. Control*, vol. 2, no. 1, pp. 6–28, Jan. 1996.
[7] J. Sottile, F. C. Trutt, and A. W. Leedy, "Condition monitoring of brushless three-phase synchronous generators with stator winding or rotor circuit deterioration," *IEEE Trans. Ind. Appl.*, vol. 42, no. 5, pp. 1209–1215, Sep. 2006.
[8] T. Zouaghi and M. Poloujadoff, "Modeling of polyphase brushless exciter behavior for failing diode operation," *IEEE Trans. Energy Convers.*, vol. 13, no. 3, pp. 214–220, Sep. 1998.
[9] C. Huang, H. W. Yuan, and Z. Ma, "The fault diagnosis of aircraft power system based on inverse problem of fuzzy optimization," *J. Aerosp. Eng.*, vol. 230, no. 6, pp. 155–175, 2016.
[10] A. Tantawy, X. Koutsoukos, and G. Biswas, "Aircraft power generators: Hybrid modeling and simulation for fault detection," *IEEE Trans. Aerosp. Electron. Syst.*, vol. 48, no. 1, pp. 552–571, Jan. 2012.
[11] Y. Li and C. Zhang, "Simulation of harmonic armature reaction in synchronous brushless excitation," in *Proc. 2nd Int. Conf. Artif. Intell., Manage. Sci. Electron. Commerce (AIMSEC)*, Aug. 2011, pp. 4304–4306.
[12] M. G. McArdle and D. J. Morrow, "Noninvasive detection of brushless exciter rotating diode failure," *IEEE Trans. Energy Convers.*, vol. 19, no. 2, pp. 378–383, Jun. 2004.
[13] J. Y. Liu, K. Gao, and P. F. Liu, "Design and application for fault monitoring circuit of rotating rectifier in aviation brushless AC generator," in *Proc. IEEE Chin. Guid., Navigat. Control Conf.*, Yantai, China, 2014, pp. 387–402.
[14] M. Salah, K. Bacha, and A. Chaari, "Detection of brushless exciter rotating diodes failures by spectral analysis of main output voltage," in *Proc. Int. Conf. Electr. Eng. Softw. Appl.*, Hammamet, Tunisia, Mar. 2013, pp. 1–6.
[15] M. Salah, K. Bacha, A. Chaari, and M. E. H. Benbouzid, "Brushless three-phase synchronous generator under rotating diode failure conditions," *IEEE Trans. Energy Convers.*, vol. 29, no. 3, pp. 594–601, Sep. 2014.
[16] D. Gray, Z. Zhang, C. Apostoaia, and C. Xu, "A neural network based approach for the detection of faults in the brushless excitation of a synchronous motor," in *Proc. IEEE Int. Conf. Electro/Inf. Technol.*, Jun. 2009, pp. 423–428.
[17] F. Rufus, S. Lee, A. Thakker, S. A. Field, and N. Kumbar, "Advanced diagnostics of aircraft electrical generators," *SAE Int. J. Aerosp.*, vol. 1, no. 1, pp. 1064–1070, Nov. 2008.
[18] J. Cui, G. Shi, and Z. Zhang, "Fault detection of aircraft generator rotating rectifier based on SAE and SVDD method," in *Proc. Prognostics Syst. Health Manage. Conf. (PHM-Harbin)*, Jul. 2017, pp. 1–5.
[19] P. C. Kjaer, T. Kjellqvist, and C. Delaloye, "Estimation of field current in vector-controlled synchronous machine variable-speed drives employing brushless asynchronous exciters," *IEEE Trans. Ind. Appl.*, vol. 41, no. 3, pp. 834–840, May 2005.
[20] Z. Wei, W. Liu, J. Pang, C. Sun, Z. Zhang, and P. Ma, "Fault diagnosis of rotating rectifier based on waveform distortion and polarity of current," in *Proc. IEEE Ind. Appl. Soc. Annu. Meeting (IAS)*, Jan. 2018, pp. 1–8.
[21] C. Sun, W. Liu, Z. Wei, N. Jiao, and J. Pang, "Open-circuit fault diagnosis of rotating rectifier by analyzing the exciter armature current," *IEEE Trans. Power Electron.*, vol. 35, no. 6, pp. 6373–6385, Jun. 2020.
[22] Z. Wei, W. Liu, J. Pang, N. Jiao, and C. Sun, "Open circuit fault diagnosis of rotating rectifier based on the polarity and symmetry of armature current," in *Proc. IEEE Energy Convers. Congr. Expo. (ECCE)*, Sep. 2018, pp. 1770–1775.
[23] C. Sun, W. Liu, X. Han, N. Jiao, K. Shen, R. Wang, S. Mao, and K. Wang, "Fault diagnosis of a rotating rectifier in a wound-rotor synchronous starter/generator in the generation mode," *IEEE Trans. Transport. Electrific.*, early access, Oct. 5, 2021, doi: 10.1109/TTE.2021.3117786.
[24] N. Jiao, X. Han, Z. Wei, C. Sun, P. Liang, and W. Liu, "Online fault diagnosis for rotating rectifier in wound-rotor synchronous starter–generator based on geometric features of current trajectory," *IEEE Trans. Ind. Electron.*, vol. 68, no. 4, pp. 2952–2963, Apr. 2021.

PEIRONG ZHU received the B.Sc. degree from Air Force Engineering University, in 2018, where he is currently pursuing the M.Sc. degree. His main research interest includes aviation electrical system health management.

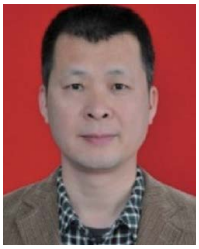

YONGZHI LIU received the B.Sc. and Ph.D. degrees from Air Force Engineering University, in 1996 and 2013, respectively. He is currently a Professor with Air Force Engineering University. His main research interests include modeling and analysis of avionics systems and health management of avionics systems.

BINGJIE FAN is currently an Associate Professor with Air Force Engineering University. Her main research includes integration of electromechanical systems and the analysis of chaotic behavior of electromechanical systems.